11th International Symposium on Turbulence and Shear Flow Phenomena (TSFP11)
Southampton, UK, July 30 to August 2, 2019

CONVECTIVE VELOCITIES OF VORTICITY FLUCTUATIONS IN TURBULENT CHANNEL FLOWS: AN INPUT-OUTPUT APPROACH

Chang Liu
Department of Mechanical Engineering
Johns Hopkins University
3400 N. Charles St. Baltimore, MD, 21218, U.S.A.
changliu@jhu.edu

Dennice F. Gayme
Department of Mechanical Engineering
Johns Hopkins University
3400 N. Charles St. Baltimore, MD, 21218, U.S.A.
dennice@jhu.edu

ABSTRACT

In this work, we analyze the convective velocities of vorticity fluctuations using an input-output approach. We first demonstrate that the convective velocities obtained in this manner reproduce known trends for both velocity and vorticity fluctuations. We then exploit the analytical framework to isolate the contributions of different scale structures to the local convective velocity of the vorticity fluctuations at different wall-normal locations. Finally, we investigate the contribution of different physical processes captured through the different terms in the linearized momentum equation. We use this term by term analysis to understand the mechanisms that lead to the deviation of the convective velocity from the mean velocity in different regions of the flow. This analysis highlights the role of viscosity, particularly in relation to the large channel spanning structures whose influence has been associated with the higher convective velocity (relative to the local mean) of structures in the near-wall region.

INTRODUCTION

Convective velocity provides an important tool to correlate spatio-temporal relationships in experiments (Dennis & Nickels, 2008) and in parametrizations of turbulence models (He *et al.*, 2017). Recent advances in computational power has enabled detailed convective velocity computations and analysis using spatially resolved Direct Numerical Simulation (DNS) data (del Álamo & Jiménez, 2009; Geng *et al.*, 2015; Renard & Deck, 2015). These studies have shed new light on this classical problem by highlighting its dependence on both streamwise and spanwise length scales. In parallel, additional insights have been gained through quantifying convective velocity using data from spatially resolved Particle Image Velocimetry (PIV) measurements (LeHew *et al.*, 2011) and two point hot-wire measurements (de Kat & Ganapathisubramani, 2015).

Convective velocity is known to deviate from the local mean velocity in the near-wall region (Lin, 1953; Krogstad *et al.*, 1998; del Álamo & Jiménez, 2009; Geng *et al.*, 2015). This larger convective velocity near the wall has been attributed to fast streamwise elongated structures (del Álamo & Jiménez, 2009) coherent up to the core region. Kim & Hussain (1993) refer to these structures as quasi-streamwise vortices. This explanation supports the notion that scale interactions provide the underlying mechanisms for the behavior of the convective velocity at the wall.

We recently employed an input-output based approach to perform detailed analysis of the scale interactions contributing to the convective velocity at different wall-normal locations in turbulent channel flow (Liu & Gayme, 2018). Related analysis based on the stochastically forced Linearized Navier-Stokes (LNS) has been widely employed to study wall-bounded shear flows; successfully uncovering flow structures leading to the largest energy amplification with respect to stochastic disturbances (Farrell & Ioannou, 1993; Bamieh & Dahleh, 2001), isolating the most sensitive input-output paths (Jovanović & Bamieh, 2005) and characterizing the role of coherent structures (McKeon & Sharma, 2010). The spatio-temporal mean convective velocity has also been computed using LNS based models with a turbulent base flow (Moarref *et al.*, 2013), and colored stochastic forcing informed by the flow statistics (Zare *et al.*, 2017). Our previous work (Liu & Gayme, 2018) expanded on the scope of the analysis in these prior studies by investigating the full streamwise-spanwise scale dependent convective velocity field. The results of that work, which focused on the convective velocity of streamwise velocity fluctuations, demonstrated good agreement with the DNS based analysis of Geng *et al.* (2015). However, we were also able to exploit the spatial-temporal transfer function to isolate the role of different scales at each wall-normal location and perform a term by term analysis of the contribution of each linear mechanism over the range of scales. In this work, we build upon these previous results by performing an analogous study of the convective velocity of vorticity fluctuations.

Understanding the transport of vortical structures and how it is affected through interactions across spatial scales is of wide interest because vortical structures and vorticity are widely used in both conceptual and predictive models of wall-bounded turbulent flows. For example, Perry *et al.* (1986) proposed Λ-shaped vortices as a candidate form for the attached eddy model (Marusic & Monty, 2019), which successfully reproduced statistical flow features such as the mean velocity and Reynolds stress profiles. Robinson (1991) similarly proposed a model based on vortical structures, including quasi-streamwise vortices and arch-like vortices, to represent turbulence production through sweep and ejection in low Reynolds number flows. Hairpin vortices packets are also the basis of the conceptual description of transport mechanisms of vorticity, momentum, and turbulent kinetic energy proposed by Adrian (2007).

Streamwise vortices, in particular, have arisen as an important example of the coherent structures that have been shown to play a key role in the dynamics of wall-bounded turbulence; see e.g., McKeon & Sharma (2010). Streamwise vortices were also demonstrated to be optimal perturbations (Butler & Farrell, 1993) and to be associated with the largest energy amplification (Bamieh & Dahleh, 2001; Jovanović & Bamieh, 2005) in channel flow. These structures have also been associated with the high skin-friction regions that are of engineering interest in wall-bounded turbulent flows (Kim, 2011).

Although there is a large body of work pointing to the importance of vorticity transport, there has yet to be a detailed analysis of scale dependent convective velocities for vorticity fluctuations. Here we adapt our input-output approach to bridge this gap by characterizing convective velocities of vorticity fluctuations in a turbulent channel. The convective velocities obtained using the proposed model reproduce trends previously observed in the literature. As in our previous analysis (Liu & Gayme, 2018), we exploit the analytical framework to isolate the contribution of each scale and linear mechanism to the deviation of the local convective velocity from the mean velocity at that wall-normal location. A term by term analysis indicates that the viscous term has a slightly larger contribution to convective velocity of streamwise vorticity than the mean shear in the viscous sublayer. Our results suggest that it is through this term that the large channel spanning structures influence the near-wall region.

In the next section, we describe the problem setup and computational method. We then present the results, followed by concluding remarks including a discussion of directions of ongoing work.

PROBLEM SETUP

We consider incompressible channel flow where x, y, z are the streamwise, wall-normal, and spanwise directions, respectively. We decompose the velocity field, $\mathbf{u} = \begin{bmatrix} u & v & w \end{bmatrix}^\mathsf{T}$, and the pressure field, p, into mean and fluctuating components; i.e., $\mathbf{u} = \bar{u}(y)\hat{\mathbf{i}} + \mathbf{u}'$ and $p = \bar{p} + p'$, where the overbars indicate time averages, $\bar{\phi} = \lim_{T\to\infty} \frac{1}{T}\int_0^T \phi(t)\,dt$, and primes indicate fluctuating quantities. We further assume invariance to shifts in (x, z, t), which allows us to use the (x, z, t) spatio-temporal Fourier transform to decompose the flow into traveling waves with wavelengths, λ_x, λ_z, and downstream phase speeds, $c = -\omega/k_x$. The associated governing equation for velocity fluctuations can be written as:

$$\underbrace{\mathrm{i}k_x(\bar{u}-c)\hat{\mathbf{u}}'}_{\mathrm{I}} \underbrace{+\hat{v}'\frac{d\bar{u}}{dy}\mathbf{i} + \hat{\nabla}\hat{p}' - \frac{1}{Re_\tau}\hat{\Delta}\hat{\mathbf{u}}'}_{\mathrm{II}} = \underbrace{\hat{\mathbf{f}}'}_{\mathrm{III}}, \tag{1a}$$

$$\hat{\nabla}\cdot\hat{\mathbf{u}}' = 0. \tag{1b}$$

Here, transformed variables are indicated with a hat. Velocity is normalized by the friction velocity; i.e., $u^+ = u_*/U_\tau$, and spatial variables are normalized by the channel half height, $y = y_*/\delta$. The friction Reynolds number is defined as $Re_\tau = \delta U_\tau/\nu = \delta^+$, where the superscript $+$ denotes variables measured in inner units. Note that we drop the superscript $+$ on the velocity vectors in (1) and what follows for ease of exposition.

The term (I) in equation (1a) describes advection of the fluctuations by the mean, while the terms in (II) include the effects of shear, pressure, and viscosity. Term (III) represents the Fourier transform of the nonlinear fluctuation-fluctuation interactions. Taylor's frozen turbulence hypothesis states that for sufficiently low turbulence intensities, turbulent fluctuations can be described as downstream advection by the mean velocity $\bar{u}(y)$, which is equivalent to setting the terms (II) and (III) in equation (1a) to zero.

We now derive the input/output response that we will use to compute the convective velocities. Equations (1a) and (1b) can be rewritten as:

$$\mathscr{L}\begin{bmatrix}\hat{\mathbf{u}}' \\ \hat{p}'\end{bmatrix} = \mathscr{B}\hat{\mathbf{f}}', \tag{2}$$

where in an abuse of notation we use the same symbol ($\mathbf{f}'$) to refer to a parametrization of the nonlinear interactions as an input forcing. In order to investigate the vorticity fluctuations, we define the following output variables:

$$\hat{\psi}' = \mathscr{C}_{\hat{\psi}'}\begin{bmatrix}\hat{\mathbf{u}}' \\ \hat{p}'\end{bmatrix}, \tag{3}$$

where $\hat{\psi}' = \hat{\omega}_x{}'$, $\hat{\omega}_y{}'$, and $\hat{\omega}_z{}'$ Here

$$\mathscr{C}_{\hat{\omega}_x{}'} = \begin{bmatrix}0 & -\mathrm{i}k_z & \partial_y & 0\end{bmatrix}, \tag{4a}$$

$$\mathscr{C}_{\hat{\omega}_y{}'} = \begin{bmatrix}\mathrm{i}k_z & 0 & -\mathrm{i}k_x & 0\end{bmatrix}, \text{ and} \tag{4b}$$

$$\mathscr{C}_{\hat{\omega}_z{}'} = \begin{bmatrix}-\partial_y & \mathrm{i}k_x & 0 & 0\end{bmatrix} \tag{4c}$$

correspond to output operators that enable one to compute the fluctuating components of the streamwise, wall-normal, and spanwise vorticity, respectively.

We then define the following input-output (I/O) map $\mathscr{G}_{\hat{\psi}'}$ between the input $\hat{\mathbf{f}}'$ and the output $\hat{\psi}'$ in the manner of, e.g., McKeon & Sharma (2010); Luhar *et al.* (2014), to yield:

$$\hat{\psi}' = \mathscr{C}_{\hat{\psi}'}\mathscr{L}^{-1}\mathscr{B}\hat{\mathbf{f}}' = \mathscr{G}_{\hat{\psi}'}(y; k_x, k_z, c)\hat{\mathbf{f}}', \tag{5}$$

which provides the fluctuating quantity $\hat{\psi}'$ at each (k_x, k_z, c) triplet for a given output map $\mathscr{C}_{\hat{\psi}'}$.

We can then compute the power spectral density using the input-output map (5) with $\mathbf{f}'(x, y, z, t)$ parametrized as spatio-temporal δ-correlated Gaussian noise with unit variance using (Jovanović & Bamieh, 2005):

$$\Phi_{\hat{\psi}'}(y; k_x, k_z, c) = \langle \hat{\psi}'\hat{\psi}'^*\rangle = \mathscr{G}_{\hat{\psi}'}\langle\hat{\mathbf{f}}'\hat{\mathbf{f}}'^*\rangle\mathscr{G}^*_{\hat{\psi}'} = \mathscr{G}_{\hat{\psi}'}\mathscr{G}^*_{\hat{\psi}'}. \tag{6}$$

Here the superscript $*$ denotes the complex conjugate, and $\langle\hat{\psi}'\hat{\psi}'^*\rangle$ indicates an ensemble average of $\hat{\psi}'\hat{\psi}'^*$.

We then compute the convective velocity of the fluctuating quantity $\hat{\psi}'$ based on a spectral generalization of the method proposed by Wills (1964) as

$$\psi_c(y; k_x, k_z) \equiv \arg\max_c \Phi_{\hat{\psi}'}(y; k_x, k_z, c). \tag{7}$$

The expression in (7) provides the convective velocities of the coherent structure with respective streamwise and spanwise wavelengths $\lambda_x = 2\pi/k_x$ and $\lambda_z = 2\pi/k_z$. This method therefore allows us to directly compute the convective velocity of the quantity of interest associated with each individual scale. We next apply this approach to investigate the convective velocity of vorticity fluctuations in turbulent channel flow.

RESULTS

The operators in (6) are discretized using the Chebyshev differentiation matrices generated by the MATLAB routines of Weideman & Reddy (2000) with 122 collocation points. We used 201 uniformly spaced points for the phase speed $c^+ \in [0, 30]$ and 90×90 logarithmically spaced points in the spectral range $k_x \in [10^{-2}, 10^3]$ and $k_z \in [10^{-2}, 10^3]$. The turbulent mean velocity at $Re_\tau \approx 1000$ in (1) is obtained from the DNS of Lee & Moser (2015).

We first validate our approach by comparing the average convective velocities of velocity fluctuations obtained from the model with those computed from DNS data (Geng *et al.*, 2015). The respective output operators associated with obtaining the streamwise, wall-normal, and spanwise velocity fluctuations $\hat{\psi}' = u', v', w'$ from equation (3) are $\mathscr{C}_{\hat{u}'} = \begin{bmatrix}1 & 0 & 0 & 0\end{bmatrix}, \mathscr{C}_{\hat{v}'} = \begin{bmatrix}0 & 1 & 0 & 0\end{bmatrix}$ and $\mathscr{C}_{\hat{w}'} = \begin{bmatrix}0 & 0 & 1 & 0\end{bmatrix}$.

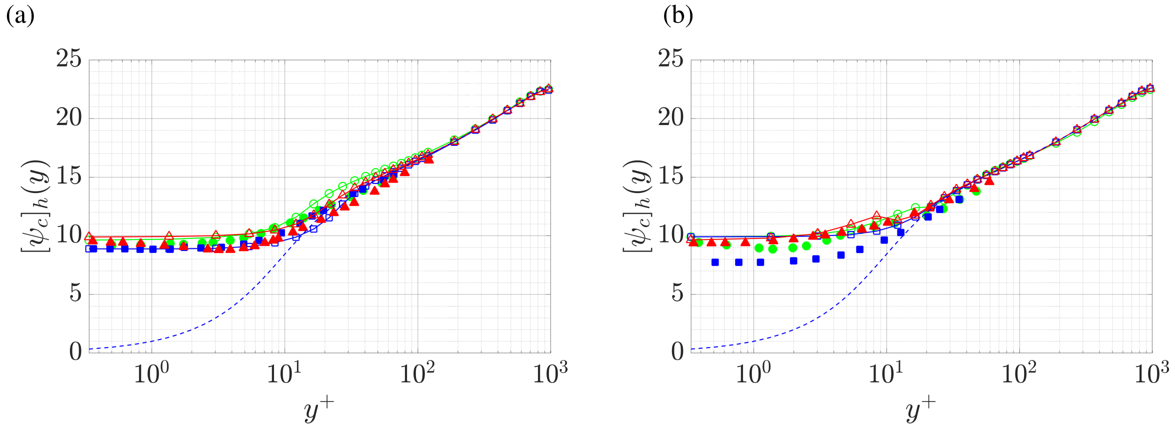

Figure 1: The average convective velocity in inner units of velocity and vorticity fluctuations, $[\psi_c]_h$: (a) $\psi = u$ (△), $\psi = v$ (□), and $\psi = w$ (○) and (b) $\psi = \omega_x$ (△), $\psi = \omega_y$ (□), and $\psi = \omega_z$ (○) with weighting function $h = \overline{|\mathscr{F}_{xz}(\psi')|^2} k_x^2$ and averaging domain $(\lambda_x^+, \lambda_z^+) > (500, 80)$ obtained from the model at $Re_\tau \approx 1000$. Results are plotted with convective velocities computed from DNS data (Geng *et al.*, 2015) at $Re_\tau = 932$: (a) $\psi = u$ (▲), $\psi = v$ (■), and $\psi = w$ (●) and (b) $\psi = \omega_x$ (▲), $\psi = \omega_y$ (■), and $\psi = \omega_z$ (●). The blue dashed lines in both (a) and (b) indicate the mean velocity profile at $Re_\tau \approx 1000$ from Lee & Moser (2015), which is used in equation (1).

The average convective velocities for each quantity $\hat{\psi}'$ are computed as:

$$[\psi_c]_h(y) = \frac{\int_\Omega \psi_c(y; k_x, k_z) h(y; k_x, k_z)\, \mathrm{d}k_x \mathrm{d}k_z}{\int_\Omega h(y; k_x, k_z)\, \mathrm{d}k_x \mathrm{d}k_z}, \qquad (8)$$

where Ω is the averaging domain and $h(y; k_x, k_z) = \langle |\mathscr{F}_{xz}(\psi')|^2 \rangle k_x^2$ is a weighting function. This weighting function is obtained from del Álamo & Jiménez (2009), who showed that it leads to values equivalent to a least squares fit to the passive advection model: $\partial_t \psi' + \psi_c \partial_x \psi' = 0$.

We specify an averaging domain $\Omega : (\lambda_x^+, \lambda_z^+) > (500, 80)$ for our model-based results in order to include the effect of sublayer streaks proposed as the source of the elevated near-wall convective velocity (Kim & Hussain, 1993), while eliminating the very small scales where nonlinear interactions dominate (and our model is not expected to be valid). Figure 1 (a) compares the average convective velocities of streamwise, wall-normal, and spanwise velocity fluctuations with those computed from DNS data by Geng *et al.* (2015), whose computations employed a least squares fit to the passive advection model. The average convective velocities of vorticity fluctuations are compared with those computed from DNS (Geng *et al.*, 2015) in Figure 1 (b). We note that convective velocities of the streamwise and spanwise vorticity components, which correspond to important flow dynamics such as the self-sustaining process, (see e.g., Waleffe (1997)), match results computed from DNS data well, while we over predict the wall-normal component.

Previous studies of convective velocities of both velocity and vorticity fluctuations show that large scale structures have higher convective velocities than the local mean velocity in the near-wall region (Kim & Hussain, 1993; Krogstad *et al.*, 1998; del Álamo & Jiménez, 2009). We now employ the model to investigate this scale dependence by examining the convective velocity at different wall-normal locations as a function of streamwise and spanwise wavelengths. Figure 2 (a) shows the convective velocities of streamwise vorticity fluctuations normalized by the local mean velocity: $\omega_{xc}(y; k_x, k_z)/\bar{u}(y)$ as a function of the streamwise-spanwise wavelengths $(\lambda_x^+, \lambda_z^+)$ in the viscous sublayer ($y^+ \approx 5$), the buffer layer ($y^+ \approx 16$), and the log-law region ($y^+ \approx 96$). The corresponding scale dependent convective velocities for the wall-normal and spanwise vorticity fluctuations are shown in figures 2 (b) and (c), respectively. In each case the vorticity fluctuations are essentially convected at the mean velocity in the log-law region (right panels), while the greatest differences are seen in the near-wall region (the left panels), as expected.

del Álamo & Jiménez (2009) defined large scale structures as those with a length scale $(\lambda_x, \lambda_z) > (2, 0.4)$. To distinguish large and small scale structures, we have indicated this wavelength pair using black dashed lines on all plots in Figure 2. The higher convective velocity of these structures $(\lambda_x, \lambda_z) > (2, 0.4)$ is seen in both the viscous sublayer ($y^+ \approx 5$) and the buffer layer ($y^+ \approx 16$) (left and center panels) with convective velocities of these structures exceeding 3.5 times the mean flow in the viscous sublayer. The penetration of these structures into the near-wall region (Kim & Hussain, 1993; del Álamo & Jiménez, 2009) has been posited as the mechanism leading to the convective velocities of fluctuating quantities exceeding the mean velocity near the wall.

The scale dependent convective velocity results in Figure 2 indicate the influence of fast moving structures centered further away from the wall, but with a footprint very near the wall due to their large size (Hutchins *et al.*, 2011). These large wavelength structures predicted through the input-output mapping employed here resemble the large, channel-filling modes of Bullock *et al.* (1978). This connection was also proposed by del Álamo & Jiménez (2009) based on their finding that u_c at the largest wavelengths is coherent throughout the channel. Our results further support their conjecture that it is the influence of these structures that leads to the breakdown of Taylor's hypothesis in the near-wall region. Further analysis of this phenomena is the subject of ongoing work.

We next use the input-output framework to further analyze the contribution of different linear mechanisms to the convective velocity of the vorticity fluctuations. The linearized equation of streamwise vorticity fluctuations is

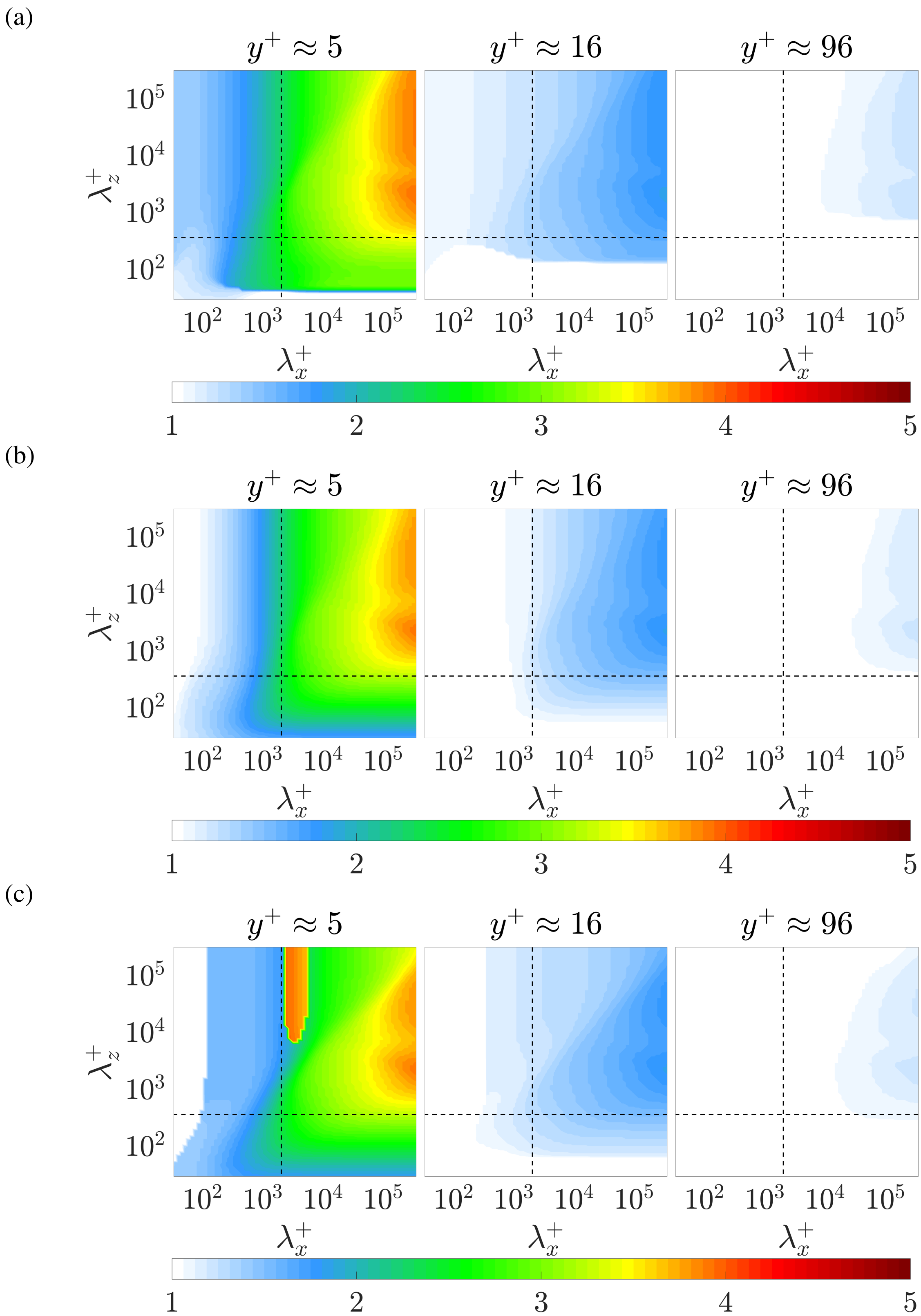

Figure 2: Scale dependent convective velocity of vorticity fluctuations at $Re_\tau = 1000$ normalized by the local mean velocity $\psi_c(y;\lambda_x,\lambda_z)/\bar{u}(y)$ in the viscous sublayer $y^+ \approx 5$, the buffer layer $y^+ \approx 16$, and the log-law region $y^+ \approx 96$. Panel (a) streamwise vorticity fluctuations $\psi = \omega_x$, (b) wall-normal vorticity fluctuations $\psi = \omega_y$, and (c) spanwise vorticity fluctuations $\psi = \omega_z$. The black dashed lines indicate the $(\lambda_x, \lambda_z) = (2, 0.4)$ cutoff for the large scales identified by del Álamo & Jiménez (2009).

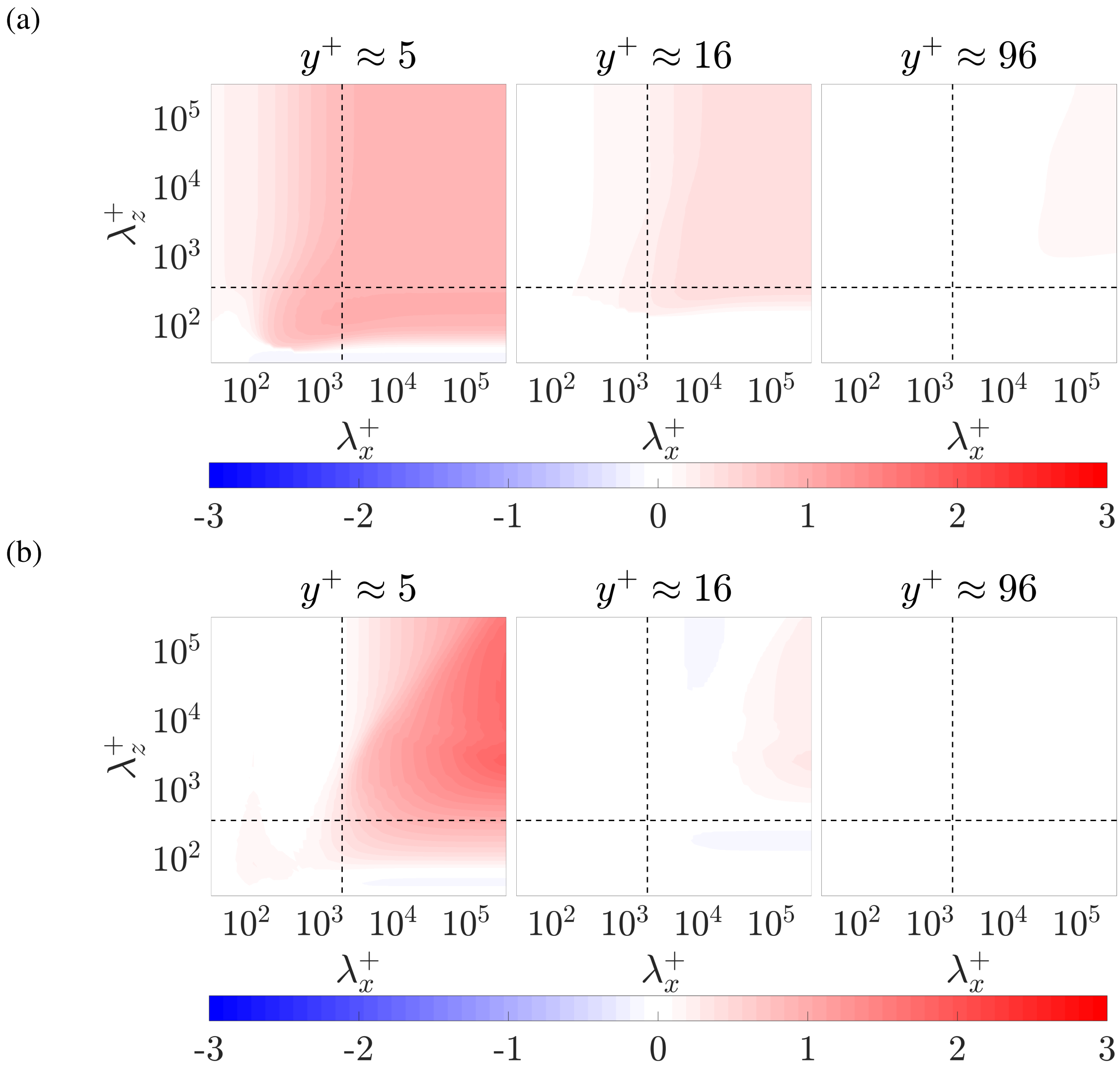

Figure 3: The deviation of convective velocity of associated with (a) the mean shear term (IIa) and (b) the viscous term (IIb) in equation (10) . All values are normalized by $k_x\bar{u}(y)\langle\hat{\omega}_x'\hat{\omega}_x'^*\rangle$, and the Reynolds number is $Re_\tau = 1000$. The black dashed lines indicate $(\lambda_x, \lambda_z) = (2, 0.4)$.

given by:

$$\mathrm{i}k_x(\bar{u}-c)\hat{\omega}_x' + \overbrace{\frac{d\bar{u}}{dy}\mathrm{i}k_x w'}^{\text{IIa}} \overbrace{-\frac{1}{Re_\tau}\hat{\Delta}\hat{\omega}_x'}^{\text{IIb}} = [\hat{\nabla}\times\hat{\boldsymbol{f}}]_x. \quad (9)$$

Here, the term (IIa) is induced by the mean shear, which represents the net effects of the tilting and stretching of the vorticity fluctuations by the mean flow and those of the mean vorticity $\nabla\times\bar{u}$ by the velocity fluctuations. Term (IIb) represents the viscous diffusion in the wall-normal direction.

We perform a similar analysis to del Álamo & Jiménez (2009) for the streamwise vorticity ω_x in equation (9). In particular, we first multiply it by $\hat{\omega}_x'^*$ and then take the imaginary part of the result to obtain the following expression for $\frac{c-\bar{u}(y)}{\bar{u}(y)}$:

$$\frac{\mathrm{Im}\left\{\overbrace{\frac{d\bar{u}}{dy}\mathrm{i}k_x\langle\hat{w}'\hat{\omega}_x'^*\rangle}^{\text{IIa}} \overbrace{-\frac{\langle\partial_{yy}\hat{\omega}_x'\hat{\omega}_x'^*\rangle}{Re_\tau}}^{\text{IIb}} - \langle[\hat{\nabla}\times\hat{\boldsymbol{f}}]_x\hat{\omega}_x'^*\rangle\right\}}{k_x\bar{u}(y)\langle\hat{\omega}_x'\hat{\omega}_x'^*\rangle}. \quad (10)$$

Equation (10) allows us to quantify each linear term's contribution to the deviation of convective velocity from the mean velocity.

In our framework, modifying the output operator allows us to directly compute the response of each of the terms in equation (10). For example, we can redefine the output operator $\mathscr{C}_{\partial^2_{yy}\hat{\omega}_x'} = \partial^2_{yy}\mathscr{C}_{\hat{\omega}_x'}$ to obtain: $\partial^2_{yy}\hat{\omega}_x'$ via equation (5). The cross-spectra $\langle\hat{w}'\hat{\omega}_x'^*\rangle$ and $\langle\partial^2_{yy}\hat{\omega}_x'\hat{\omega}_x'^*\rangle$ are then determined using a similar approach as in (6); for example:

$$\langle\hat{w}'\hat{\omega}_x'^*\rangle = \mathscr{G}_{\hat{w}'}\langle\hat{\mathbf{f}}'\hat{\mathbf{f}}'^*\rangle\mathscr{G}^*_{\hat{\omega}_x'} = \mathscr{G}_{\hat{w}'}\mathscr{G}^*_{\hat{\omega}_x'}. \quad (11)$$

Figures 3 (a) and (b) show the respective contribution from the mean shear term (IIa) and the viscous term (IIb) to the convective velocity of the streamwise vorticity fluctuations. The results indicate that the mean shear contributes slightly more to the deviation of the convective velocity from the mean than the viscous term in the buffer layer ($y^+ \approx 16$). However, in the viscous sublayer ($y^+ \approx 5$), the viscous term provides a relatively larger contribution to the deviation of the convective velocity from the mean than the mean shear, which is similar to the authors observations regarding the streamwise velocity fluctuations. The term (IIa) may be estimated as $\sim O(C/y)$, while the term (IIb) as $\sim O(C/y^2)$. This estimation suggests that the viscous diffusion effect is decreasing faster than the mean shear as the distance from the wall increases, but the viscous diffusion is more important as we approach the wall. This is consistent with the observation in Figure 3.

CONCLUSIONS

In this work, we apply an input-output model to analyze convective velocities of vorticity fluctuations in a turbulent channel. The average and scale dependent convective velocities obtained using the proposed model reproduce the mean trends previously observed in the literature. Our approach further allows us to isolate the contribution of each scale and linear mechanism to the deviation of convective velocity from the local mean, thereby providing insight into the underlying flow dynamics. A term by term analysis indicates that the viscous term has a slightly larger contribution to the convective velocity of streamwise vorticity than the mean shear but that it is this term that captures the influence of large scale structures on the near-wall region. This analysis suggests that including an additional viscous term in Taylor's hypothesis has the potential to capture the effect of large scale structures $(\lambda_x, \lambda_z) > (2, 0.4)$ on the local convective velocity near the wall (del Álamo & Jiménez, 2009). Further analysis of the underlying mechanism and exploring associated corrections to Taylor's Hypothesis are directions of ongoing work.

ACKNOWLEDGMENTS

The authors gratefully acknowledge support from the US National Science Foundation (NSF) through grant number CBET 1652244 and the Office of Naval Research (ONR) through grant number N00014-18-1-2534. C.L. also greatly appreciates support from the Chinese Scholarship Council.

REFERENCES

Adrian, R. J. 2007 Hairpin vortex organization in wall turbulence. *Phys. Fluids* **19** (4), 041301.

Bamieh, B. & Dahleh, M. 2001 Energy amplification in channel flows with stochastic excitation. *Phys. Fluids* **13** (11), 3258–3269.

Bullock, K. J., Cooper, R. E. & Abernathy, F. H. 1978 Structural similarity in radial correlations and spectra of longitudinal velocity fluctuations in pipe flow. *J. Fluid Mech.* **88** (3), 585–608.

Butler, K. M. & Farrell, B. F. 1993 Optimal perturbations and streak spacing in wall-bounded turbulent shear flow. *Phys. Fluids A-Fluid* **5** (3), 774–777.

del Álamo, J. C. & Jiménez, J. 2009 Estimation of turbulent convection velocities and corrections to Taylor's approximation. *J. Fluid Mech.* **640**, 5–26.

Dennis, D. J. C. & Nickels, T. B. 2008 On the limitations of Taylor's hypothesis in constructing long structures in a turbulent boundary layer. *J. Fluid Mech.* **614**, 197–206.

Farrell, B. F. & Ioannou, P. J. 1993 Stochastic forcing of the linearized Navier-Stokes equations. *Phys. Fluids A-Fluid* **5** (11), 2600–2609.

Geng, C., He, G., Wang, Y., Xu, C., Lozano-Durán, A. & Wallace, J. M. 2015 Taylor's hypothesis in turbulent channel flow considered using a transport equation analysis. *Phys. Fluids* **27** (2), 025111.

He, G., Jin, G. & Yang, Y. 2017 Space-time correlations and dynamic coupling in turbulent flows. *Annu. Rev. Fluid Mech.* **49** (1), 51–70.

Hutchins, N., Monty, J. P., Ganapathisubramani, B., Ng, H. C. H. & Marusic, I. 2011 Three-dimensional conditional structure of a high-Reynolds-number turbulent boundary layer. *J. Fluid Mech.* **673**, 255–285.

Jovanović, M. R. & Bamieh, B. 2005 Componentwise energy amplification in channel flows. *J. Fluid Mech.* **534**, 145–183.

de Kat, R. & Ganapathisubramani, B. 2015 Frequency-wavenumber mapping in turbulent shear flows. *J. Fluid Mech.* **783**, 166–190.

Kim, J. 2011 Physics and control of wall turbulence for drag reduction. *Philos. Trans. Royal Soc. A* **369** (1940), 1396–1411.

Kim, J. & Hussain, F. 1993 Propagation velocity of perturbations in turbulent channel flow. *Phys. Fluids A* **5** (3), 695–706.

Krogstad, P., Kaspersen, J. H. & Rimestad, S. 1998 Convection velocities in a turbulent boundary layer. *Phys. Fluids* **10** (4), 949–957.

Lee, M. & Moser, R. D. 2015 Direct numerical simulation of turbulent channel flow up to $Re_\tau = 5200$. *J. Fluid Mech.* **774**, 395–415.

LeHew, J., Guala, M. & McKeon, B. J. 2011 A study of the three-dimensional spectral energy distribution in a zero pressure gradient turbulent boundary layer. *Exp. Fluids* **51** (4), 997–1012.

Lin, C. C. 1953 On Taylor's hypothesis and the acceleration terms in the Navier-Stokes equations. *Q. Appl. Math.* **10** (4), 295–306.

Liu, C. & Gayme, D. 2018 Input-output based analysis of convective velocity in turbulent channels. *Bull. Am. Phys. Soc., Atlanta, GA,* **63** (13).

Luhar, M., Sharma, A. S. & McKeon, B. J. 2014 On the structure and origin of pressure fluctuations in wall turbulence: predictions based on the resolvent analysis. *J. Fluid Mech.* **751**, 38–70.

Marusic, I. & Monty, J. P. 2019 Attached eddy model of wall turbulence. *Annu. Rev. Fluid Mech.* **51**, 49–74.

McKeon, B. J. & Sharma, A. S. 2010 A critical-layer framework for turbulent pipe flow. *J. Fluid Mech.* **658**, 336–382.

Moarref, R., Sharma, A. S., Tropp, J. A. & McKeon, B. J. 2013 Model-based scaling of the streamwise energy density in high-Reynolds-number turbulent channels. *J. Fluid Mech.* **734**, 275–316.

Perry, A. E., Henbest, S. & Chong, M. S. 1986 A theoretical and experimental study of wall turbulence. *J. Fluid Mech.* **165**, 163–199.

Renard, N. & Deck, S. 2015 On the scale-dependent turbulent convection velocity in a spatially developing flat plate turbulent boundary layer at Reynolds number $Re_\theta = 13000$. *J. Fluid Mech.* **775**, 105–148.

Robinson, S. K. 1991 Coherent motions in the turbulent boundary layer. *Annu. Rev. Fluid Mech.* **23** (1), 601–639.

Waleffe, F. 1997 On a self-sustaining process in shear flows. *Phys. Fluids* **9** (4), 883–900.

Weideman, J. A. C. & Reddy, S. C. 2000 A MATLAB differentiation matrix suite. *ACM Trans. Math. Softw.* **26** (4), 465–519.

Wills, J. A. B. 1964 On convection velocities in turbulent shear flows. *J. Fluid Mech.* **20** (3), 417–432.

Zare, A., Jovanović, M. R. & Georgiou, T. T. 2017 Colour of turbulence. *J. Fluid Mech.* **812**, 636–680.